Electronic Supplementary Material (ESI) for Soft Matter.

Journal Name

ARTICLE TYPE

Cite this: DOI: 00.0000/xxxxxxxxxx

Multistable Interaction between a Spherical Brownian Particle and an Air-Water Interface

Stefano Villa,[a] Antonio Stocco,[b] Christophe Blanc,[a] and Maurizio Nobili*[a]

Received Date
Accepted Date

DOI: 00.0000/xxxxxxxxxx

S1 Resolution in the gap distance measurement

The RIM basic model (BM) considers only incident and reflected rays parallel to the optical axis. Within this model the particle-interface gap distance d can be computed from the location of an extremum located near the center of the pattern (see Eq.2 and related text). The uncertainty σ_d on d then derives from the propagation of the errors on the radius, σ_a, and on the position of the extremum with respect to the center of the interference pattern, σ_{r_e}:

$$\sigma_d = \sqrt{\left(\frac{\partial d}{\partial r_e}\sigma_{r_e}\right)^2 + \left(\frac{\partial d}{\partial a}\sigma_a\right)^2} = \sqrt{\frac{r_e^2\sigma_{r_e}^2}{a^2 - r_e^2} + \left(\frac{a}{\sqrt{a^2 - r_e^2}} - 1\right)^2 \sigma_a^2} \tag{S1}$$

The error on the radius a is of the order of 50 nm, while the one on the position of the extremum σ_{r_e} is given by the sum of two sources:

$$\sigma_{r_e} = \sigma_{par} + \sigma_c \tag{S2}$$

The first term is the error in the determination of r_e obtained from a parabolic fit of the light intensity close to the extremum. It results in $\sigma_{par} = 10$ nm. The second term σ_c is related to the error δ_{xy} in the measurement of the center of the interference pattern. The evaluation of σ_c can be made computing from the analytical expression of the interference pattern $I(x,y,z)$ the φ-averaged intensity profile centered on a new point located at a distance δ_{xy} from the center of the fringe system. From this radial profile the coordinate $\tilde{r}_e$ of an extremum is calculated. It can be shown that $\tilde{r}_e$ is related to r_e by the relation*:

$$\tilde{r}_e = \frac{\delta_{xy}}{2\pi}\int_0^{2\pi}\sqrt{\frac{r_e^2}{\delta_{xy}^2} - \sin^2\varphi}\, d\varphi \tag{S3}$$

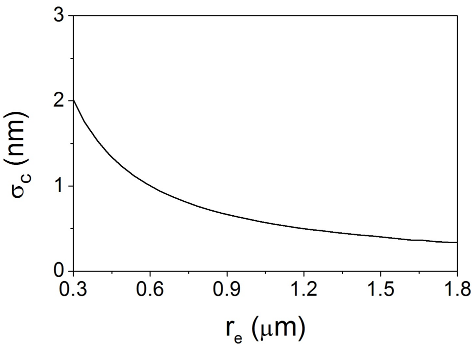

Fig. S1 Error on r_e related to the error of the measurement of the interference pattern center.

The value of $\sigma_c = |r_e - \tilde{r}_e|$ evaluated for $\delta_{xy} = \sigma_{xy} = 0.05$ μm is reported in Fig.S1 as a function of r_e. Since the range of r_e considered in the analysis is between 0.5 and 1.5 μm, it can be seen that the contribution of σ_c to the total error on r is in the nanometric range and negligible if compared to σ_{par}.

Considering all sources of error on r_e and a, the resulting error on d evaluated with equation S1 is of the order of 10 nm for the typically considered extrema located at 1 μm from the center of the interference pattern and in any considered case lower than 20 nm.

We have discussed the main sources of errors within BM but the adequacy of this model with the experimental data can also

---

[a] Laboratoire Charles Coulomb (L2C), University of Montpellier, CNRS, Montpellier, France. E-mail: maurizio.nobili@umontpellier.fr

[b] Institut Charles Sadron (ICS), University of Strasbourg, CNRS, Strasbourg, France.

[*] In order to simplify the problem, calculations are made supposing a simplified I equal to 1 for $r = r_e$ and equal to 0 elsewhere. This simplification allows the determination of the upper limit of the error. Since the resulting error is negligible compared to other sources of incertitude, no more refined evaluations are necessary.

be questioned. The contrast of the patterns shown in Fig.4 of the Main Text (MT) decreases with the distance from the center and obviously departs from what Eq. 1 of MT predicts. As already examined by different authors, several corrections indeed have to be included to quantitatively explain the intensity observed in RIM (see an example in ref [11] of MT). Colloidal spherical beads have then been studied as model systems and comparisons between measurements and models have been extensively discussed (reference [12] of MT). Apart from the decreasing contrast, a slightly stretched fringe spacing is also observed. Both features are satisfactorily handled when refined theories of RICM image formation are used. The presence of tilted rays (finite aperture) and their reflection on the curved surface of the microsphere should be taken into account. BM indeed considers only incident and reflected rays parallel to the optical axis. Experimentally, a finite numerical aperture of the objective implies the presence of tilted incident rays (which incoherently interfere). Moreover the curvature of the bead modifies the tilt of the reflected rays depending on the point of incidence of the rays on the surface. Both phenomena were included in a numerical computation of the interference pattern due to a bead. Refractive indexes of water, air and polystyrene are used to compute the polarisation-dependant Fresnel coefficients at the various interfaces, the fields and optical paths differences of all pairs of rays such as the one shown in Fig.S2a. The resulting intensity distribution satisfactory fits the measured intensity (see Fig. S2b). Such a refined model (RM) gives a slightly larger particle-interface gap with respect to the direct application of BM. For the considered beads (from R=3.5μm to 6μm) and gap distances from 150nm to 400nm, the two methods, however, gives a systematic difference of 10-20nm, comparable to the experimental error discussed above.

S2 Fitted values of radii and Debye screening lengths

In section 3.2 of the main text is described the fit of the experimental potential wells around d_0^I. The free fitting parameters are the air-water interface potential, an additive constant energy, the particle radius a and the Debye screening length λ_D. The resulting fitted values of the interface potential are discussed in the main text. Concerning a and λ_D, a comparison can be done between the fitted values and the expected results. In figure S3a the ratio between the best fitting radii a_{fit} found for sulfate spheres and the corresponding radii a_{meas} measured from particle's bright field image are given as a function of a_{meas}. Similarly, in fig. S3b the ratio between the best fitting Debye lengths $\lambda_{D,fit}$ found for sulfate spheres and the corresponding expected values $\lambda_{D,exp}$ known from sample's molarity are given as a function of $\lambda_{D,exp}$. The found values for the radii are on average greater by a factor 1.09 than the measured ones. Small variations of the radius affect the potential mostly on its attractive branch, where gravity dominates: fits made fixing $a = a_{meas}$, indeed, returns same values of ψ_{AL} and λ_D. The ratio $\lambda_{D,fit}/\lambda_{D,exp}$, close to 1 at low λ_D, progressively decreases to about 0.5 as the ions concentration is reduced. Such trend can be explained considering, as reported in the main text, that the Debye screening length holds for linearized Poisson-

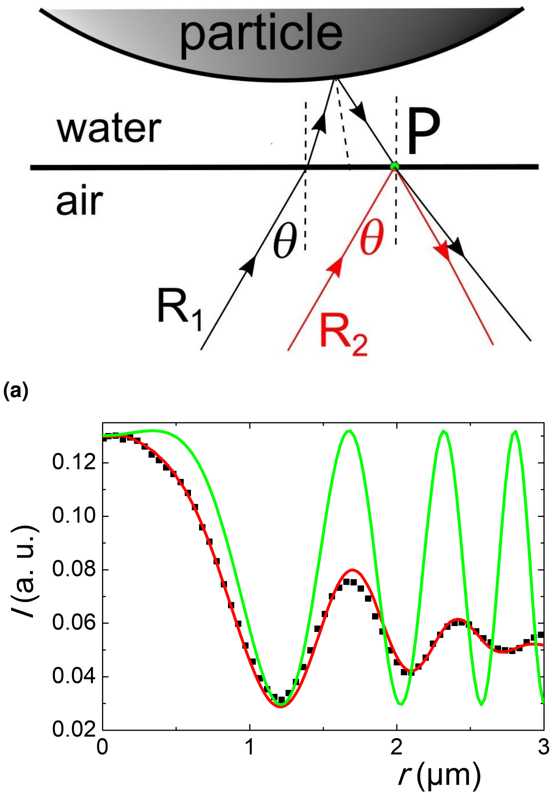

(a)

(b)

Fig. S2 a) Example of two tilted rays R_1 and R_2 interfering at P in the observation plane. The tilt θ is limited by the numerical aperture of the incident rays. The objective numerical aperture also bounds the tilt of the re-entering rays. b) Symbols: typical intensity distribution represented as a function of the distance r from the pattern center (angular integration for a polystyrene bead of radius $a = 5.85\mu$m). The contrast decreases rapidly with r. The plain red curve corresponds to the RM intensity computed with the following parameters: wavelength $\lambda = 625$nm, refractive indexes $n_a = 1$ (air), $n_w = 1.33$ (water) and n_{PS}=1.59 (Polystyrene), numerical aperture NA=0.6 for both incident and reflected rays. The best fit shown here gives $d \approx 241$nm. For comparison, we have also plotted (plain green curve) the intensity that would give BM for the gap $d \approx 225$nm predicted from the location of the first black fringe. A discrepancy of about 16nm is present in the measurement of the gap between the two methods.

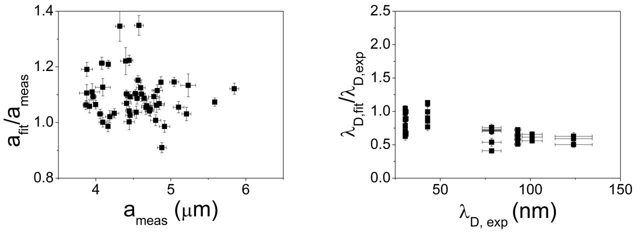

(a)

(b)

Fig. S3 Sulfate spheres: (a) Same particle ratio a_{fit}/a_{meas} between the particle radius a_{fit} obtained from the fit of ΔU^I and the one measured a_{meas} from the particle's bright field image versus a_{meas}. (b) Ratio $\lambda_{D,fit}/\lambda_{D,exp}$ between the Debye screening length $\lambda_{D,fit}$ obtained from the fit of ΔU^I and the one $\lambda_{D,exp}$ calculated from the solution's molarity versus $\lambda_{D,exp}$.

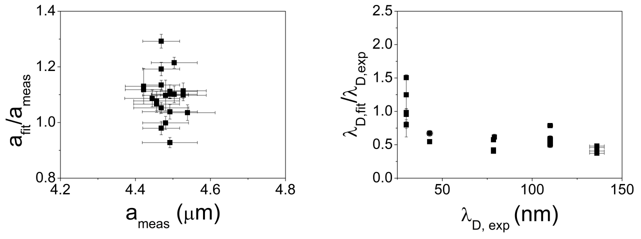

(a) **(b)**

Fig. S4 Carboxylated spheres: (a) Same particle ratio a_{fit}/a_{meas} between the particle radius a_{fit} obtained from the fit of ΔU^I and the one measured a_{meas} from the particle's bright field image versus a_{meas}. (b) Ratio $\lambda_{D,fit}/\lambda_{D,exp}$ between the Debye screening length $\lambda_{D,fit}$ obtained from the fit of ΔU^I and the corresponding expected one $\lambda_{D,exp}$ calculated from the solution's molarity versus $\lambda_{D,exp}$.

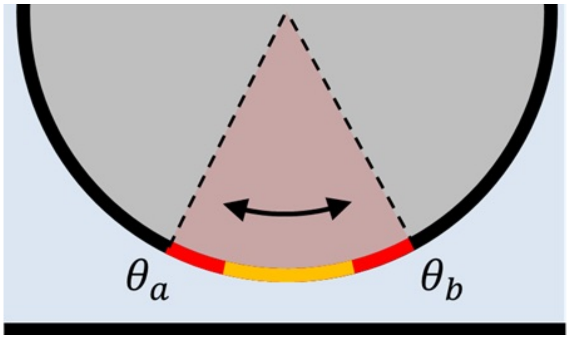

(a)

Fig. S5 Sketch of the particle in the second equilibrium position with the range $[\theta_a, \theta_b]$ of the angular fluctuations of the heterogeneity (yellow line) stressed by the red area. The range covers two times the size of the heterogeneity.

Boltzmann (PB) equation i.e. for $e\psi/k_BT \ll 1$. Because of the experimental value of $e\psi/k_BT$ higher than one, PB linearization results in a not well defined λ_D. This explanation is supported by the better agreement observed at high molarities, when the error made linearizing PB is lower.

Figure S4 reports for the carboxylated spheres the same ratios (a_{fit}/a_{meas} (a) and $\lambda_{D,fit}/\lambda_{D,exp}$ (b)) as in fig. S3. The trends are the same as the ones of the sulfate spheres for both the radius and the Debye length. In agreement with the information provided by the producers, the carboxylated particles are much more monodisperse than the sulfate ones.

S3 Evaluation of size and number of heterogeneities

In the main text is reported the estimated value of the size and the mutual distance of the heterogeneities present on the surface of a particle. The size of the heterogeneities is estimated from the particle angular fluctuations in the second minimum supposing an heterogeneity-interface interaction which decays fast enough so that its contribution is negligible when the heterogeneity is not turned towards the interface. Defining $[\theta_a, \theta_b]$ the range of angles covered by θ when the particle is in the second equilibrium position, the typical heterogeneity size results in $\ell = a\,|\theta_a - \theta_b|/2$.

particle ID	ℓ from σ_θ (nm)
1	50
2	20
3	40

Table S1 Average size of the heterogeneities evaluated for three different particles from the fluctuations of θ in the second equilibrium position. They are recovered considering a rectangular potential well having a width corresponding to the standard deviation σ_θ of the distribution of angles.

The angular amplitude $|\theta_a - \theta_b|$ has been evaluated as the standard deviation σ_θ of the Gaussian distribution of θ. As it can be seen from Table S1 the obtained sizes are of the order of tens of nanometers.

In order to make the transition from the first equilibrium position to the second one a particle has to rotationally diffuse until it exposes one heterogeneity towards the interface. The mean distance between heterogeneities can be evaluated from the measurement of the particle rotational diffusion time and the known value of the rotational diffusion coefficient close to the interface.

The rotational diffusion time corresponds to the residence time in the first minimum. Unfortunately, it is difficult to access to this time with our experimental setup as the small field of view coupled with the low employed particle density prevents the full tracking of most of the particles from the arrival at the first minimum until the transition to the second minimum. Consequently, only a rough estimation based on qualitative observations can be made. In the experiments at $c \geq 10^{-4}$ M, the majority of particles are found in the second equilibrium position after a time interval $\tau = 30$ minutes from the complete sedimentation of the sample to the interface. Considering a rotational diffusion coefficient of $D_{rot} = 1.4 \cdot 10^{-3}$ s^{-1} (ref. [28] of the main text), which corresponds to a particle at the first minimum (particle-interface typical distance of $d = 0.04a$), the typical angle $\Delta\theta_{het}$ the particle have to rotate before to orient an heterogeneity toward the interface can be estimated as

$$\Delta\theta_{het} \sim \sqrt{4 D_{rot} \tau} \sim 180^\circ \tag{S4}$$

Such value implies that just one heterogeneity per particle is sufficient to provoke the transition between the first and the second minimum.

S4 Solution degassing

In order to probe the role of air nanobubbles in the particle- interface interaction we have compared the behavior of degassed samples with the one measured in normal conditions. In particular, we measure at a given time t from sample preparation the number of particles residing in one of the two equilibria compared to the total number of particles. The ratio between such two numbers gives the time dependent probability to find a particle in the bulk and not adsorbed at the interface; lower is this ratio larger is the probability of adsorption at the interface. Since, as reported in the main text, the interface breaching is related to the existence of the measured second equilibrium, the calculated probability for

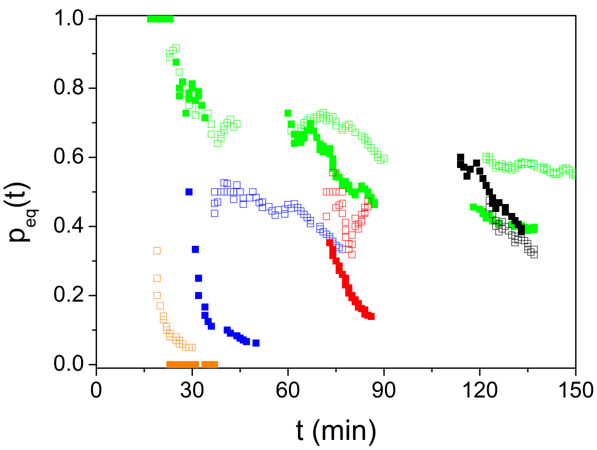

Fig. S6 Measured probabilities of occupancy of one of the two equilibria as a function of time ($t = 0$ is the sample preparation time) for not degassed (plain squares) and degassed (void squares) samples. Different colors refer to different samples all prepared at 10^{-4} M. The probability $p_{eq}(t) = N_{eq}(t)/N_{tot}(t)$ at time t is evaluated by dividing the number of particles in the bulk (showing an interference pattern) by the total number of observed particles.

both normal and degassed samples allows to address the role of air bubble in its appearance. We look at such probability because of its immediacy[†] compared to the time consuming tracking and data analysis described in the main text required for the discrimination between the first and the second equilibrium position.

In the experiment a mother particle solution is divided in two batches; one batch is observed in normal conditions, the other one is degassed for 30 minutes in a vacuum desiccator. In figure S6 is reported versus time the ratio between the number of particles fluctuating around a minimum and the total number of observed particles. Time $t = 0$ corresponds to the sample preparation, while different colors refer to different samples. Plain squares are for degassed samples, open squares for samples in normal conditions. In all samples the number of particle remaining in solution close to the interface decreases with time as more and more particles get adsorbed at the interface. Such trapping dynamics is significantly dependent on the degassing. Despite the great variability from the considered sample, on average in degassed samples particles remain longer in solution with respect to particles in normal samples. Such results point out the important role of air bubbles in the particle trapping dynamics at the interface and therefore suggest that air-bubble may also play a role in the appearance of the related second equilibrium position.

[†] The discrimination between a particle located in one of the equilibria and the adsorbed particles is straightforward because of the absence of the interference pattern in the latter case.